

High-fidelity pseudopotentials for the contact interaction

P. O. Bagnion, P. López Ríos, R. J. Needs, and G. J. Conduit

Cavendish Laboratory, J.J. Thomson Avenue, Cambridge CB3 0HE, United Kingdom

(Received 5 June 2014; published 24 September 2014)

The contact interaction is often used in modeling ultracold atomic gases, although it leads to pathological behavior arising from the divergence of the many-body wave function when two particles coalesce. This makes it difficult to use this model interaction in quantum Monte Carlo and other popular numerical methods. Researchers therefore model the contact interaction with pseudopotentials, such as the square well potential, whose scattering properties deviate markedly from those of the contact potential. In this article, we propose a family of pseudopotentials that reproduce the scattering phase shifts of the contact interaction up to a hundred times more accurately than the square well potential. Moreover, the pseudopotentials are smooth, resulting in significant improvements in efficiency when used in numerical calculations.

DOI: [10.1103/PhysRevA.90.033626](https://doi.org/10.1103/PhysRevA.90.033626)

PACS number(s): 03.75.Hh, 71.15.Dx, 31.15.A–

I. INTRODUCTION

Interactions between particles are central to our understanding of correlated phenomena. The contact potential is often used to model interactions in ultracold atomic gases but, despite its widespread use, it displays pathological behavior: both the potential and wave function diverge when two particles coalesce. These divergences impede numerical methods and are commonly handled by replacing the contact potential by a pseudopotential, such as a hard sphere or a square well potential. However, these approximations to the contact potential display incorrect variations in the scattering phase shift with incident particle energy [1–6]. In this article, we adapt methods commonly used for the development of electron-ion pseudopotentials in the electronic structure community to propose an atom-atom pseudopotential whose scattering properties agree closely with those of the contact interaction.

Ultracold atomic gases have delivered many important insights into strongly correlated systems. They can both provide clean model Hamiltonians and introduce the ability to tune the strength of the contact interactions. Ultracold atoms interact through an underlying attractive van der Waals interaction. An external magnetic field can be used to tune the energy of the bound molecular state to approach the energy of the scattering state, causing the states to couple resonantly. The effect of the resonance on the scattering state can be modeled by an effective interparticle potential [7]. In the case of broad Feshbach resonances, the scattering can be described by a single universal scattering length a which describes the scattering phase shift arising from a contact interaction. There are three types of contact interaction: sufficiently deep to trap a two-body bound state ($a > 0$), weakly attractive with no bound state ($a < 0$), and repulsive (excited state of the $a > 0$ potential).

Contemporary numerical simulations of the first two types, the bound state ($a > 0$) and weak attractive interactions ($a < 0$), normally adopt a finite-ranged square well or Pöschl-Teller interaction. Such simulations have delivered crucial insights into Bose gases [2] and the crossover from a gas of weakly coupled Bardeen-Cooper-Schrieffer pairs to a strongly interacting Bose-Einstein condensate [1,8], as well as few-atom physics [9–11]. However, the finite range imbues the potential with incorrect scattering properties. Reducing

the range of the potential alleviates this problem, but slows numerical calculations.

The third type of contact potential gives repulsive interactions that drive itinerant ferromagnetism in Fermi gases [4,5,12], a Tonks-Girardeau gas [1], and a Bose gas [6]. The repulsive interaction emerges from the first excited state of the bound-state potential. Both the repulsive contact potential and the bound-state potential therefore have $a > 0$. In ultracold atomic gas experiments [13] the excited state (also called the upper branch) is protected from decay to the ground state by a slow three-body loss process, allowing the study of repulsive interactions. To simulate these repulsive interactions, one can adopt a finite-ranged attractive potential and study the first excited eigenstate [4,5]. However, studying excited states in quantum Monte Carlo (QMC) methods often requires restricting the excited-state wave function to be orthogonal to the lower energy states. Variational estimates of excited-state energies calculated within the widely used diffusion quantum Monte Carlo (DMC) method [14–16] are discussed in Ref. [17]. The fixed node constraint used in the DMC method prevents collapse into the ground state, but it is still difficult to calculate reliable excited-state energies within the framework of DMC. An alternative approach is to use a repulsive top-hat potential [12] whose ground state resembles the first excited state of the contact potential. However, this potential has a finite range greater than the scattering length, resulting in an incorrect scattering phase shift.

The difficulty in simulating repulsive interactions means that there are important open questions about fermionic gases: Is the ground state of a strongly interacting fermionic system ferromagnetic [3,12,18–23]? Is the ferromagnetic transition first or second order? And do exotic phases emerge around the quantum criticality such as spin spirals [12], nematic phases [21,24,25], and a counterintuitive p -wave superconducting state [26–32]? The development of a pseudopotential that is better able to reproduce the scattering properties of the contact interaction will help resolve these open questions.

In Sec. II, we present two pseudopotentials for the interatomic interaction in a cold atom gas. We first adapt norm-conserving pseudopotentials [33–35], developed by the electronic structure community for electron-ion interactions, to deal effectively with scattering states. We then present a pseudopotential constructed to minimize the scattering phase

shift error for all wave vectors in a Fermi gas. In Sec. III, we test the accuracy of the proposed formalism using the exactly soluble system of two trapped atoms. In Sec. IV, we investigate how the pseudopotential performs in a many-body setting by calculating the equation of state of the weakly repulsive Fermi gas and comparing results to a perturbation expansion.

II. DERIVATION OF THE PSEUDOPOTENTIALS

To construct the pseudopotential we study the two-body problem: two identical fermions in their center-of-mass frame with wave vector $k \geq 0$. The Hamiltonian in atomic units ($\hbar = m = 1$) in the center of mass frame is

$$-\frac{\nabla^2}{2\mu}\psi + V(\mathbf{r})\psi = \frac{k^2}{2\mu}\psi,$$

where $V(\mathbf{r}) = 4\pi a\delta(\mathbf{r})(\partial/\partial r)r$ is the contact potential for scattering length a and interparticle separation \mathbf{r} [36], and $\mu = 1/2$ is the reduced mass.

The scattering states for the contact potential are $\psi_{k,\ell}^{\text{cont}} = \sin[kr - \ell\pi/2 + \delta_\ell^{\text{cont}}(k)]/kr$, where

$$\delta_\ell^{\text{cont}}(k) = \begin{cases} \arctan(-ka), & \ell = 0, \\ 0, & \ell > 0, \end{cases}$$

is the scattering phase shift in the angular momentum channel ℓ . We seek a pseudopotential that

(1) reproduces the correct phase shifts over the range of wave vectors $0 \leq k \lesssim k_F$ present in a Fermi gas with Fermi wave vector k_F ,

(2) supports no superfluous bound states to be compatible with ground state methods, and

(3) is smooth to accelerate numerical calculations.

We start by developing pseudopotentials for the repulsive branch, then the attractive branch, and finally the bound state. When developing pseudopotentials, we benchmark their quality by looking at how closely the phase shift of the wave function for the relative motion of two particles interacting via the pseudopotential reproduces the phase shift of the contact interaction for all wave vectors $0 \leq k \lesssim k_F$ present in a Fermi gas, as shown in Figs. 2 and 3.

A. Repulsive branch

We first focus on developing a pseudopotential for the repulsive branch of the contact interaction. This branch offers a particular challenge. The bare potential is strongly attractive, harboring exactly one bound state, as shown in Fig. 1(a). The excited states of this potential must maintain orthogonality to the bound state, resulting in a positive phase shift. The scattering states have one more node than the noninteracting state with the same wave vector, as shown in Fig. 1(a).

We describe four families of pseudopotentials: hard sphere, soft sphere (top hat), the Troullier-Martins form of norm-conserving pseudopotential [33,37], and a pseudopotential that aims to minimize the error in the scattering phase shift over all wave vectors occupied in the Fermi gas. The first two families (the hard sphere and top hat) have frequently been

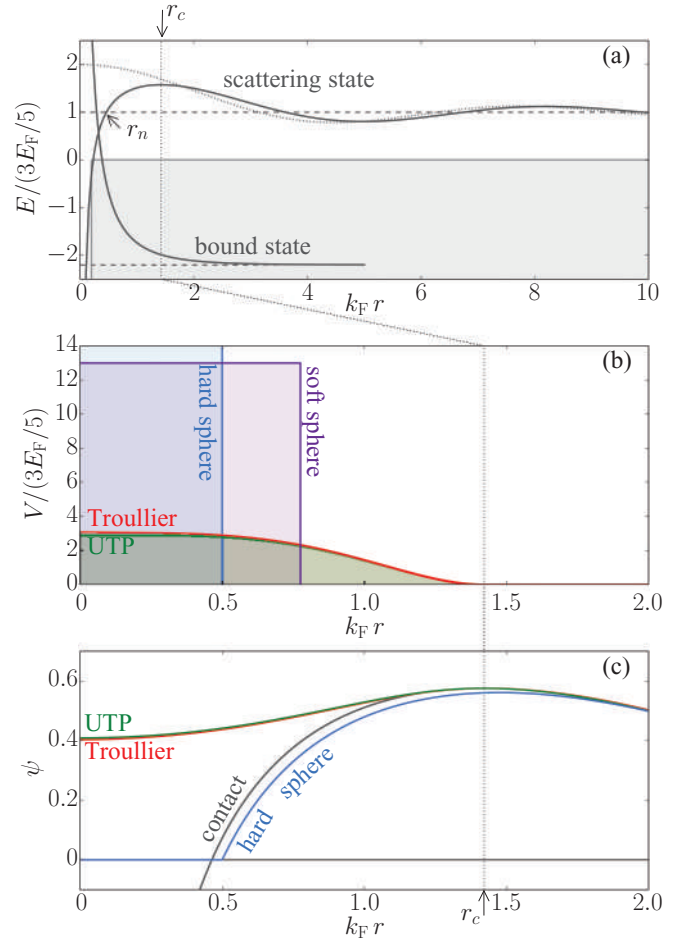


FIG. 1. (Color online) (a) Bound- and scattering-state wave functions for contact interactions at $k_F a = 0.5$, offset by their respective eigenvalues (dashed lines) as a function of interparticle separation. The bare contact potential (represented by the gray area) is strongly attractive and harbors a single bound state. The scattering states incident on the potential incur a positive phase shift with respect to the noninteracting scattering wave function (dotted line). r_n denotes the first node of the scattering wave function and r_c denotes the first antinode, which we use as the cutoff radius when constructing pseudopotentials, as described in Sec. II A. (b) The pseudopotentials at $k_F a = 1/2$ on the repulsive branch. The potential labeled “Troullier” denotes the pseudopotential derived using the Troullier-Martins formalism. The line labeled “UTP” denotes the pseudopotential derived using the UTP formalism. These formalisms are described in Sec. II. (c) The wave functions for the relative motion of two particles interacting with a contact potential, the hard sphere, Troullier-Martins pseudopotential, and UTP, at $k = k_F$.

used as approximations to the contact potential in numerical calculations [3–5,11,12].

The usual approach [4,12] to the construction of pseudopotentials for the contact interaction starts from the low-energy expansion for the s -wave scattering phase shift,

$$\cot \delta_0(k) = -\frac{1}{ka} + \frac{1}{2}kr_{\text{eff}} - Pr_{\text{eff}}^3 k^3 + O(k^5), \quad (1)$$

where r_{eff} is the “effective range” of the potential and P is the “shape parameter.” For a contact potential, r_{eff} and all higher

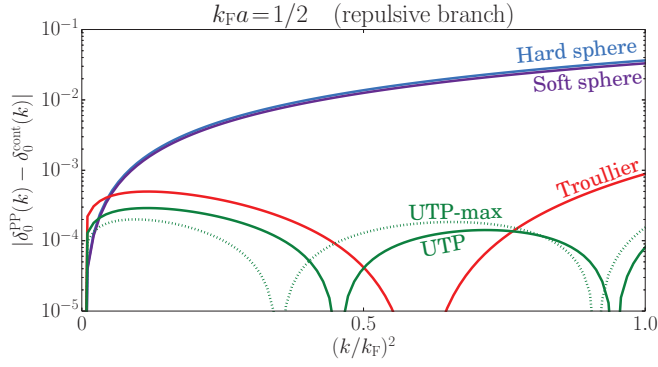


FIG. 2. (Color online) The errors in phase shifts $|\delta_0^{\text{PP}}(k) - \delta_0^{\text{cont}}(k)|$ for the repulsive branch at $k_F a = 1/2$. δ_0^{cont} is the s -wave scattering phase shift for the contact interaction and δ_0^{PP} is the scattering phase shift for each of the pseudopotentials. The Troullier-Martins formalism is approximately two orders of magnitude more accurate than the hard and soft-sphere pseudopotentials commonly used as approximations to the contact interaction. The UTP formalism offers an additional factor of 2 improvement. The dotted green line labeled UTP-max denotes the phase-shift error of a variant of the UTP developed by minimizing the peak phase-shift error.

order terms are zero. Perhaps the simplest pseudopotential is a hard-sphere potential with radius a . This reproduces the correct scattering length a , thereby delivering the correct phase shift for $k = 0$. However, the hard sphere has an effective range $r_{\text{eff}} = 2a/3$. To study the impact of the pseudopotential on the scattering states, we calculate the phase shifts at $k_F a = 1/2$ for all wave vectors between 0 and k_F and compare them to the contact phase shifts. Figure 2 shows that the finite effective range of the hard-sphere potential causes significant deviations in the scattering phase shift for $k > 0$.

To reduce the error in the scattering phase shift, Ref. [12] adopted a soft-sphere potential: $V(r) = V_0 \Theta(r - R)$, with V_0 and R chosen to reproduce the contact scattering length $a = R(1 - \tanh \gamma/\gamma)$ and effective range $r_{\text{eff}} = R[1 + \frac{3 \tanh \gamma - \gamma(3 + \gamma^2)}{3\gamma(\gamma - \tanh \gamma)^2}] = 0$, where $\gamma = R\sqrt{2\mu V_0}$. The first two terms in the low-energy expansion of the phase shift are now correct, leading to a small reduction in phase-shift error as shown in Fig. 2.

The two potentials considered so far display incorrect behavior at large wave vectors due to the focus on reproducing the correct $k = 0$ scattering behavior. To improve the accuracy we turn to the Troullier-Martins [37] formalism developed for constructing attractive electron-ion pseudopotentials [33–35, 38–40]. These pseudopotentials reproduce both the correct phase shift and its derivative with respect to energy at a prescribed calibration energy. The Troullier-Martins form of norm-conserving pseudopotential can readily be applied to the construction of a pseudopotential for the contact interaction. We choose a calibration energy and cutoff radius as follows:

Calibration energy. The pseudopotential will have scattering properties identical to the contact potential at the calibration energy. For electron-ion pseudopotentials, the bound-state energy in an isolated ion is a natural choice.

For example, in a homogeneous fermionic gas the scattering of states with incident momenta less than $\sim k_F$ is particularly important, and therefore we choose a calibration energy equal to the median energy of the occupied states, $(3/5)E_F$.

Cutoff radius. The Troullier-Martins pseudo-wave-function is identical to the contact wave function outside of the cutoff radius, but has no nodes inside the cutoff radius, as shown in Fig. 1(c). We can therefore choose the cutoff radius to eliminate the bound state: by selecting a radius $r_c > r_n$, where r_n is the position of the first node in the wave function, we construct a pseudopotential that does not have a bound state, as shown in Fig. 1(b). We choose the first antinode of the wave function at the calibration energy as the cutoff radius for the pseudopotential.

Having chosen a suitable calibration energy and cutoff radius, we construct the pseudo-wave-function. The contact potential exhibits a nonzero phase shift only when the particles are incident with angular momentum quantum number $\ell = 0$. We therefore concentrate on reproducing the correct $\ell = 0$ behavior in this section. We demonstrate how to eliminate scattering in higher angular momentum channels in Sec. II D.

The functional form of the pseudo-wave-function in the $\ell = 0$ channel at the calibration energy is

$$\psi^{\text{PP}}(\mathbf{r}) = \begin{cases} \exp\left(\sum_{i=0}^6 c_i r^{2i}\right) Y_0(\theta, \phi), & r < r_c, \\ \psi_{k, \ell=0}^{\text{cont}}(r), & r \geq r_c, \end{cases}$$

where $k = \sqrt{(3/5)E_F}$ is the wave vector at the calibration energy and $\mathbf{r} = (r, \theta, \phi)$ is the relative position of the interacting particles. The coefficients c_i are calculated by demanding continuity of the pseudo-wave-function and its first four derivatives at the cutoff radius, and requiring that the derivative of the phase shift with respect to energy, $\partial(\cot \delta)/\partial E|_{(3/5)E_F}$, be the same as that of the contact interaction at the calibration energy. This last condition, called the norm-conservation condition, is equivalent to demanding that the total density enclosed by $r < r_c$ for the pseudo-wave-function matches that of the contact wave function,

$$\int_{|\mathbf{r}| < r_c} |\psi^{\text{PP}}(\mathbf{r})|^2 d\mathbf{r} = \int_{|\mathbf{r}| < r_c} |\psi_{k, \ell=0}^{\text{cont}}(\mathbf{r})|^2 d\mathbf{r}.$$

Finally, we demand that $c_2^2 = -5c_4$, to guarantee that the pseudopotential has zero curvature at the origin. Having constructed the pseudo-wave-function at the calibration energy, we invert the Schrödinger equation to obtain the pseudopotential $V^{\text{PP}}(r)$. The formalism for the contact interaction is detailed in the Appendix. We also provide a computer program to generate the pseudopotential [41].

By calibrating the pseudopotential at the median incident scattering energy $E = (3/5)E_F$, we reduce the error in the scattering phase shift over a broad range of wave vectors. This generates the pseudopotential shown in Fig. 1(b), whose smoothness leads to improved numerical stability and efficiency. Figure 2 demonstrates that this potential is exact at the calibration energy $E = (3/5)E_F$ and delivers a hundredfold decrease in phase-shift error across all wave vectors, compared to the soft-sphere pseudopotential.

The Troullier-Martins formalism yields a pseudopotential that reproduces the contact behavior exactly at the calibration energy, but deviates at other energies. One approach for reducing the deviation is to ensure that higher order derivatives of the phase shift with respect to energy are equal to those of the contact interaction. A second option is to impose accurate scattering at multiple energies through additional parameters.

$$\frac{V(r)}{E_F} = \begin{cases} (1 - \frac{r}{r_c})^2 [v_1(\frac{1}{2} + \frac{r}{r_c}) + \sum_{i=2}^{N_v} v_i(\frac{r}{r_c})^i], & r \leq r_c, \\ 0, & r > r_c, \end{cases}$$

with $N_v = 9$. The term $(1 - r/r_c)^2$ ensures that the potential goes smoothly to zero at $r = r_c$ and the term $v_1(1/2 + r/r_c)$ constrains the potential to have zero gradient at $r = 0$ to allow the pseudo-wave-function to be as smooth as possible. This is advantageous in quantum chemistry methods in which the absence of a cusp improves convergence with respect to the basis set size. As with the Troullier-Martins pseudopotential, we choose a cutoff radius that corresponds to the first antinode of the true wave function, removing the node at $r = r_n$ and therefore eliminating the bound state. To calculate the coefficients $\{v_i\}$, we minimize the total squared error in the phase shift over all wave vectors between 0 and k_F ,

$$\langle (\delta_\ell^{\text{PP}} - \delta_\ell^{\text{cont}})^2 \rangle = \frac{\int_0^{k_F} [\delta_\ell^{\text{PP}}(k) - \delta_\ell^{\text{cont}}(k)]^2 w(k) dk}{\int_0^{k_F} w(k) dk},$$

where the phase shift $\delta_\ell^{\text{PP}}(k)$ is determined from a numerical calculation of the scattering solution of the pseudopotential and $w(k) = k^2$ is a positive weighting function. We include a computer program to generate the UTP in the supplemental material [41]. The computer program starts with coefficients determined from the Troullier-Martins pseudopotential, but we verified that the optimization was not stuck in a local minimum by repeating the process with different initial coefficients.

As demonstrated in Fig. 2, this potential gives an error in δ_0 of less than 10^{-3} for all wave vectors $0 \leq k \leq k_F$ found in a Fermi gas, corresponding to an improvement of two orders of magnitude over previously used pseudopotentials, and an approximate twofold improvement over the Troullier-Martins pseudopotential.

We test the robustness of the UTP construction by generating two additional variants of the formalism. The first, inspired by the Troullier-Martins pseudopotential, contains only even terms in the polynomial functional form of the potential. For the second variant, rather than minimizing the total squared phase-shift error $\int_0^{k_F} [\delta_\ell^{\text{PP}}(k) - \delta_\ell^{\text{cont}}(k)]^2 w(k) dk$, we instead minimize the maximum phase-shift error $\max_{0 \leq k \leq k_F} (|\delta_\ell^{\text{PP}}(k) - \delta_\ell^{\text{cont}}(k)|)$. Including only even terms in the polynomial functional form of the pseudopotential delivers a 1% poorer quality pseudopotential for the same number of variational parameters. Minimizing the maximum phase-shift error leads to a similar pseudopotential, with a slightly smaller peak error, but the phase shifts deviate more from those of the contact interaction elsewhere. Ultimately the selection of the optimization strategy depends on the physics of the system: for density waves one should minimize the error

Here we pursue the natural conclusion of these approaches by constructing a pseudopotential that minimizes the error in the phase shifts over all the wave vectors occupied in a Fermi gas. We derive this pseudopotential below, referring to it as an “ultratransferable pseudopotential” (UTP).

The UTP is identical to the contact potential outside of a cutoff radius r_c , but has a polynomial form inside the cutoff,

around $k = 0$, while for s -wave superconductivity one should minimize the error around $k = k_F$. However, having verified that different optimization procedures lead to similar high-quality pseudopotentials, we continue with the optimization of the total squared phase-shift error.

B. Attractive branch

We can use a similar procedure to derive Troullier-Martins and ultratransferable pseudopotentials for the attractive branch, $a < 0$. The main difference from the repulsive branch lies in the choice of cutoff: for the repulsive branch, the cutoff must lie beyond the first node of the wave function, while for the attractive branch there is no lower bound on the cutoff.

The smaller the cutoff, the closer the scattering properties of the pseudopotential approach those of the contact potential. However, reducing the cutoff comes at the cost of computational efficiency. For example, in quantum Monte Carlo simulations, the sampling efficiency of a potential is proportional to the fraction of configuration space volume in which the potential is finite, r_c^3/Ω , where Ω is the simulation cell volume.

In Fig. 3(a) we adopt a cutoff $r_c = 1/2k_F$, and compare the results to the square well potential with cutoff $r_c = 0.01\sqrt[3]{3\pi^2}/k_F$ used in Ref. [1]. Both the Troullier-Martins pseudopotential and the UTP have an average error approximately 10 times smaller than the square well potential, but their larger cutoff allows them to be sampled 4000 times more efficiently in QMC. Reducing the cutoff used for the Troullier-Martins pseudopotential or the UTP would further increase their accuracy, at the cost of a reduction in sampling efficiency.

In Fig. 3(b), we compare the phase-shift accuracy of the pseudopotentials as a function of cutoff. Both the Troullier-Martins and ultratransferable formalisms result in pseudopotentials whose scattering phase shifts converge to those of the contact interaction considerably faster than the square well potential. We find that the average error in phase shift of both the Troullier-Martins pseudopotential and UTP tends to zero as r_c^3 . By contrast, the square well converges as r_c . The improved convergence can be understood as a consequence of imposing norm-conservation, which guarantees the correctness of $\partial(\cot \delta)/\partial E|_{(3/5)E_F}$ around the calibration energy $(3/5)E_F$. Equation (1) then shows that the leading error in the phase shifts is approximately proportional to

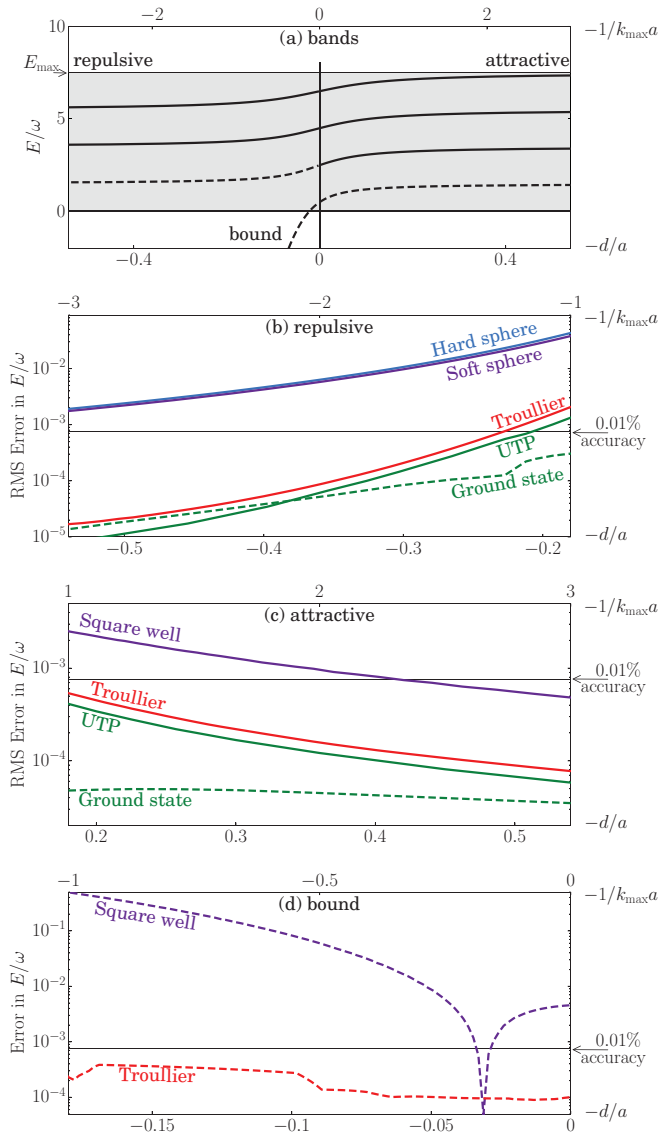


FIG. 4. (Color online) (a) Band diagram for two atoms in a harmonic trap, calculated following Ref. [36]. (b) Mean-squared error in total energy for two atoms in a harmonic trap, for all bands below E_{\max} (solid lines), for repulsive interactions ($k_{\max}a > 0$). UTP denotes the ultratransferable pseudopotential. The dashed line denotes the error in the ground-state energy with the UTP. The labels $-d/a$ and $-1/k_{\max}a$ describe the x axis, which can be interpreted as either a change in trap size for constant interaction strength (varying d/a where $d = 1/\sqrt{\omega}$), or a change in interaction strength for constant trap size (varying $1/k_{\max}a$, where $k_{\max} = \sqrt{E_{\max}}$). The horizontal solid black line shows the typical many-body accuracy goal of 0.01%. (c) The pseudopotential error for attractive interactions ($k_{\max}a < 0$). (d) The pseudopotential error in the bound-state energy.

the Troullier-Martins and ultratransferable pseudopotentials [shown in Figs. 4(b) and 4(c)] are significantly more accurate, each giving an error smaller than $\sim 0.01\%$. For the attractive branch, we could have created more accurate pseudopotentials by decreasing the cutoff r_c , as demonstrated in Fig. 3(b). Finally we examine the bound-state energy in Fig. 4(d). Both the square well and Troullier-Martins formalism give

the exact ground-state energy for two atoms in a vacuum. However, the trapping potential introduces inhomogeneity, and the square well potential gives a $\sim 10\%$ error in the ground-state energy, whereas the Troullier-Martins pseudopotential delivers errors of less than $\sim 0.01\%$. This affirms the benefits of using a pseudopotential that is robust against changes in the local environment. The success of the Troullier-Martins and ultratransferable formalisms in describing the ground state is all the more significant considering that these pseudopotentials aim to describe the correct scattering properties over a range of energies. We would therefore expect them to perform even better when modeling the excited states of the trap.

B. Excited states

We now examine the predictions for the excited states in the repulsive and attractive branches. Due to the shell structure, the excited states of a few-body system are related to the ground state of a many-body system [9], allowing us to probe the performance expected from the pseudopotential in a many-body setting. We consider states up to a maximum energy of $E_{\max} = 7.5\hbar\omega$, corresponding to 112 noninteracting atoms in the trap. In Figs. 4(b) and 4(c) the Troullier-Martins pseudopotential has a mean-squared error averaged over all bands below E_{\max} between 10 and 100 times lower than the hard sphere and square well pseudopotentials. The UTP is a further factor of 2 more accurate. Additionally, when modeling the attractive branch, the Troullier-Martins and ultratransferable formalisms produce pseudopotentials that converge to the contact limit more rapidly than the attractive square well, resulting in improved efficiency when used in a QMC simulation. For the cutoff radii used in Fig. 4(c), using the Troullier-Martins pseudopotentials or the UTP results in QMC calculations that are 4000 times more efficient than the equivalent calculation with the square well.

The pseudopotentials deliver energies with better than $\sim 0.01\%$ accuracy, a significant improvement over existing pseudopotentials. This means that they are no longer the limiting factor in studies of ultracold atomic gases with state-of-the-art computational methods. For example, exact diagonalization calculations have been performed at a similar $\sim 0.01\%$ accuracy [11], and high-fidelity many-body QMC can also achieve $\sim 0.01\%$ stochastic error [3–5]. We are therefore well positioned to test the pseudopotential in a many-body setting.

IV. CASE STUDY: FERMI GAS

Having demonstrated the efficacy of the Troullier-Martins and UTP formalisms for an inhomogeneous two-body system, we now test the pseudopotentials using quantum Monte Carlo methods. We calculate the equation of state of a Fermi gas with weak interactions. Fermi gases serve as models for free electrons in a conductor, for nucleons inside a large nucleus, and for liquid He³ [50].

For the attractive Fermi gas, the quality of a pseudopotential can be systematically improved by reducing the cutoff radius. We therefore concentrate on the repulsive branch of the Feshbach resonance, for which the top-hat pseudopotential cannot be systematically improved. We compare the energies

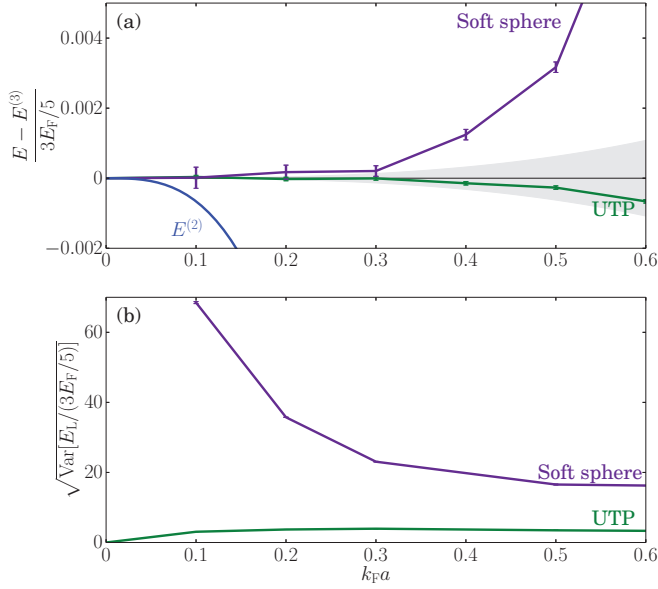


FIG. 5. (Color online) (a) Deviation of the equation of state from that predicted by third-order perturbation theory, as given by Eq. (2). The gray region denotes the confidence intervals in $E^{(3)}$. The line denoted $E^{(2)}$ is the equation of state derived from second-order perturbation theory [59]. We note that the equation of state obtained by using a soft-sphere pseudopotential deviates significantly from the line predicted by the perturbation expansion. (b) Standard deviation of the local energy E_L for the ground state of the soft sphere and the UTP. The soft-sphere pseudopotential exhibits a much larger standard deviation, which can be explained by the abrupt changes in potential energy when particles overlap.

predicted by DMC calculations with exact perturbation expansions calculated with the contact potential. The main result is shown in Fig. 5: energies calculated using the UTP and top hat differ significantly for $k_F a \gtrsim 0.3$. The equation of state calculated using the UTP formalism agrees well with third-order perturbation theory, confirming the accuracy of the formalism.

A. Formalism

We use the DMC method [14–16], as implemented in the CASINO code [51] with a Slater-Jastrow trial wave function and a backflow transformation [52]. The wave function takes the form $\Psi = e^J D_\uparrow D_\downarrow$, where D_\uparrow and D_\downarrow are Slater determinants of plane-wave orbitals for each of the spin channels. The Jastrow factor e^J describes the interparticle correlation

$$J = \sum_{\substack{j \neq i \\ \alpha, \beta \in \{\uparrow, \downarrow\}}} \left(1 - \frac{|\mathbf{r}_i - \mathbf{r}_j|}{L_{\alpha\beta}^u}\right)^2 u_{\alpha\beta}(|\mathbf{r}_i - \mathbf{r}_j|) \times \Theta(L_{\alpha\beta}^u - |\mathbf{r}_i - \mathbf{r}_j|),$$

where $u_{\alpha\beta}$ is a polynomial whose parameters we optimize in a variational Monte Carlo (VMC) calculation, $L_{\alpha\beta}^u$ is a cutoff length that we also optimize variationally, and Θ is the Heaviside step function [53]. The backflow transformation

shifts electron positions in the Slater determinant as

$$\mathbf{r}_{i\sigma} \rightarrow \mathbf{r}_{i\sigma} + \sum_{\substack{j \neq i \\ \alpha, \beta \in \{\uparrow, \downarrow\}}} (\mathbf{r}_i - \mathbf{r}_j) \eta_{ij}^{\alpha\beta}(|\mathbf{r}_i - \mathbf{r}_j|),$$

where

$$\eta_{ij}^{\alpha\beta}(r) = \left(1 - \frac{r}{L_{\alpha\beta}^\eta}\right)^2 \Theta(L_{\alpha\beta}^\eta - r) p_{\alpha\beta}(r),$$

$p_{\alpha\beta}$ is a polynomial whose parameters are optimized in VMC, and $L_{\alpha\beta}^\eta$ is a cutoff length that we also optimize. The backflow transformation allows the description of further correlation, reducing the final DMC energy [5,52].

We calculate the equation of state of the Fermi gas with 81 up-spin and 81 down-spin particles. We use twist averaging [54–56] and correct the noninteracting kinetic energy with that of the corresponding infinite system [4] to reduce finite-size effects. We use a control variate method to reduce the stochastic error resulting from the twist-averaging procedure [57]. We find that the control variate method leads to a fivefold reduction in stochastic error for this system at no additional computational cost.

B. Results

We compare the equations of state of the UTP and soft-sphere pseudopotential in Fig. 5. The two differ significantly for $k_F a \gtrsim 0.3$, highlighting the importance of using an accurate pseudopotential. To establish which potential reproduces the equation of state of the contact potential more closely, we compare the results to a third-order perturbation theory calculation of the equation of state [50,58],

$$E^{(3)} = \frac{3}{5} E_F \left[1 + \frac{10}{9\pi} k_F a + \frac{4(11 - 2 \ln 2)}{21\pi^2} (k_F a)^2 + (0.076 \pm 0.005 - 1/3\pi)(k_F a)^3 \right]. \quad (2)$$

Figure 5(a) shows that the equation of state calculated using the UTP remains within the stochastic error of $E^{(3)}$ up to $k_F a \sim 0.6$. In contrast, the equation of state for the soft-sphere system deviates significantly from the perturbation result for $k_F a \gtrsim 0.3$. The energy $E^{(2)}$ obtained using second-order perturbation theory [59], which is used frequently in the literature [18,23], differs markedly from both the UTP and soft-sphere pseudopotential energy. These significant differences in energy affirm the importance of using a pseudopotential whose scattering properties accurately replicate those of the contact interaction.

In Fig. 5(b), we compare the variance in the local energy $E_L = \hat{H}\Psi/\Psi$ of the ground-state wave function for different pseudopotentials. The stochastic error for a quantum Monte Carlo calculation is proportional to $\sqrt{\text{Var}(E_L)}$. A smoother local energy will therefore result in more accurate results for the same computational expense. By virtue of its smoothness, we find that the UTP leads to smoother local energies than the soft-sphere pseudopotential. In particular, the variance of the local energy at small $k_F a$ diverges for the zero-range soft-sphere pseudopotential. Even at $k_F a = 0.6$, we find that

the standard deviation of the UTP ground state is about five times smaller than that of the soft-sphere ground state, resulting in a 25-fold improvement in efficiency in quantum Monte Carlo calculations.

The computational expense, for a fixed number of VMC or DMC samples, of all the pseudopotentials considered in this article scales as $O(N^2)$ with particle number N . This quadratic dependence arises from the need to check the separation of all pairs of particles to decide whether the particles are close enough to interact. The prefactor of this term is therefore identical for all pseudopotentials. We must therefore consider the prefactor of the $O(N)$ term to discern a difference in the computational expense of using the pseudopotentials. The square well or top hat potential scales more favorably, both because it is easier to compute the value of the pseudopotential and because, by virtue of its smaller cutoff radius, fewer pairs of particles interact. In practice, we find that for the 162-particle system considered in this section at $k_F a = 0.6$, it takes approximately 25% less CPU time to acquire the same number of VMC samples with a top-hat potential than with a UTP. This difference is far outweighed by the lower variance in local energy of the UTP: QMC calculations with a top-hat pseudopotential are approximately 19 times more costly than calculations with a UTP, to obtain the same level of accuracy.

V. DISCUSSION

We have developed a high-fidelity pseudopotential for the contact interaction inspired by pseudopotentials common in the electronic structure community. We tested the pseudopotential by examining the scattering phase shifts, the energy of two trapped particles, and the ground-state energy of a Fermi gas, finding the new pseudopotentials to be approximately 100 times more accurate for the repulsive branch, and 10 times more accurate for the attractive and bound-state branches of the Feshbach resonance, while also 4000 times more efficient than contemporary approximations. The pseudopotential delivers accurate scattering properties over all wave vectors $0 \leq k \lesssim k_F$ in a Fermi gas. Its smoothness also greatly accelerates computation: for instance, for the repulsive branch of the Feshbach resonance, calculations are accelerated by a factor of at least 19.

The performance and transferability of the pseudopotential makes it widely applicable across first-principles methods including VMC, DMC, coupled cluster, and configuration interaction methods. The formalism developed can also be applied more widely to generate pseudopotentials for narrow Feshbach resonances, the repulsive Coulomb interaction, or the dipolar interaction. The formalism could also be extended by using more projectors or the ultrasoft [46] or augmented plane-wave [47] formalisms popular in the electronic structure community.

ACKNOWLEDGMENTS

The authors thank Stefan Baur, Andrew Green, Jesper Levensen, Gunnar Möller, Michael Rutter, and Lukas Wagner for useful discussions, and acknowledge the financial support of the EPSRC and Gonville & Caius College. This research used computational resources provided by the Cambridge High

Performance Computing Service and the Argonne Leadership Computing Facility at Argonne National Laboratory. The latter is supported by the Office of Science of the US Department of Energy under Contract No. DE-AC02-06CH11357.

APPENDIX: CONSTRUCTION OF THE TROULLIER-MARTINS PSEUDOPOTENTIAL

The equations in the Troullier-Martins paper pertain to electron-ion pseudopotentials in the context of the Born-Oppenheimer approximation [37]. They therefore consider the interaction of an electron with a much heavier nucleus. By contrast, in this paper, we are interested in the interaction between two particles of equal mass. This corresponds to using a reduced mass $\mu = 1/2$ in the center-of-mass frame, rather than $\mu \simeq 1$ for electron-ion pseudopotentials. We adapt the Troullier-Martins formalism to the construction of a pseudopotential for two particles of equal mass interacting with a contact interaction.

The Schrödinger equation for relative motion with reduced mass of $1/2$ and a spherically symmetric interparticle potential is

$$[-\nabla^2 + V(\mathbf{r})]\psi_{E,\ell}(\mathbf{r}) = E\psi_{E,\ell}(\mathbf{r}),$$

where $\mathbf{r} = \mathbf{r}_1 - \mathbf{r}_2$ is the relative position of the two particles and $\psi_{E,\ell}$ is the relative wave function associated with energy eigenvalue E and angular momentum channel ℓ . We only consider particles with relative angular momentum quantum number $\ell = 0$, since the contact interaction only scatters in this channel.

By expanding the relative wave function $\psi_{E,\ell=0}(\mathbf{r}) = R_{E,\ell=0}(r)Y_0$, where $Y_0 = 1/\sqrt{4\pi}$ is the zeroth spherical harmonic and $r = |\mathbf{r}|$, we can recast the three-dimensional Schrödinger equation as a radial equation,

$$\left[-\frac{1}{r^2} \frac{\partial}{\partial r} \left(r^2 \frac{\partial}{\partial r} \right) + V(r) \right] R_{E,\ell=0} = E R_{E,\ell=0}. \quad (\text{A1})$$

We choose a calibration energy E_c , as described in the main text, and construct the pseudopotential by choosing a pseudo-wave-function that matches the exact form beyond a cutoff radius r_c , at the calibration energy. Following Troullier-Martins, we define the pseudo-wave-function at the calibration energy as $\psi_{E_c,\ell=0}^{\text{PP}} = R_{E_c,\ell=0}^{\text{PP}} Y_0$ with the radial component

$$R_{E_c,\ell=0}^{\text{PP}}(r) = \begin{cases} R_{E_c,\ell=0}^{\text{cont}}(r), & r \geq r_c, \\ \exp[p(r)], & r < r_c, \end{cases}$$

where $p(r) = \sum_{i=0}^6 c_i r^{2i}$ is a polynomial and $R_{E_c,\ell=0}^{\text{cont}}$ is the radial wave function for the contact interaction at the calibration energy E_c . Inserting this form into the radial equation, Eq. (A1), we calculate an expression for the pseudopotential V^{PP} as a function of $p(r)$,

$$V^{\text{PP}}(r) = \begin{cases} 0, & r \geq r_c, \\ E_c + p'' + p'^2 + \frac{2}{r} p', & r < r_c, \end{cases} \quad (\text{A2})$$

where the primes indicate derivatives.

To proceed further, we must consider an explicit functional form for $R_{E_c,\ell=0}^{\text{cont}}$. This depends on whether we are constructing a pseudopotential for a scattering state or the bound state

of the contact interaction. We consider these two cases in Appendices 1 and 2.

1. Scattering states

The relative wave function for two particles interacting via contact interactions is

$$R_{E,\ell=0}^{\text{cont}}(r) = \frac{\sin[kr + \delta_0(k)]}{kr},$$

where $\delta_0(k) = \arctan(-ka)$ and $k = \sqrt{E}$. The continuity equations at the cutoff are

$$p(r_c) = \ln \left\{ \frac{\sin[kr_c + \delta_0(k)]}{r_c} \right\},$$

$$p'(r_c) = \frac{k}{\tan(kr_c + \delta)} - \frac{1}{r_c},$$

$$p''(r_c) = -k^2 - \frac{2}{r_c}p' - p'^2,$$

$$p^{(3)}(r_c) = \frac{2}{r_c^2}p' - \frac{2}{r_c}p'' - 2p'p'',$$

$$p^{(4)}(r_c) = -\frac{4}{r_c^3}p' + \frac{4}{r_c^2}p'' - \frac{2}{r_c}p^{(3)} - 2p''^2 - 2p'p^{(3)},$$

where $p^{(i)}$ denotes the i th derivative of p and all derivatives are evaluated at $r = r_c$. To obtain the pseudo-wave-function at

the calibration energy, we solve this system of five equations, as well as the norm-conservation condition and impose $c_2^2 = -5c_4$ to guarantee $\partial^2 V^{\text{PP}}/\partial r^2|_{r=0} = 0$. This uniquely determines the polynomial $p(r)$, which, in turn, determines the pseudopotential, following Eq. (A2).

2. Bound state

The relative wave function for two particles in the bound state of the contact interaction is

$$R_{E,\ell=0}^{\text{cont}}(r) = \left(\frac{k^3}{2\pi} \right)^{1/2} \frac{\exp(kr)}{kr},$$

where $k = \sqrt{E}$ and $E = -1/a^2$ for scattering length a . The continuity equations at the cutoff $r = r_c$ are

$$p(r_c) = -\frac{k}{r_c} - \ln(r_c),$$

$$p'(r_c) = -k - \frac{1}{r_c},$$

$$p''(r_c) = -k^2 - \frac{2}{r_c}p' - p'^2,$$

$$p^{(3)}(r_c) = \frac{2}{r_c^2}p' - \frac{2}{r_c}p'' - 2p'p'',$$

$$p^{(4)}(r_c) = -\frac{4}{r_c^3}p' + \frac{4}{r_c^2}p'' - \frac{2}{r_c}p^{(3)} - 2p''^2 - 2p'p^{(3)}.$$

-
- [1] G. E. Astrakharchik, J. Boronat, J. Casulleras, and S. Giorgini, *Phys. Rev. Lett.* **93**, 200404 (2004).
- [2] G. E. Astrakharchik, D. Blume, S. Giorgini, and B. E. Granger, *Phys. Rev. Lett.* **92**, 030402 (2004).
- [3] G. J. Conduit, A. G. Green, and B. D. Simons, *Phys. Rev. Lett.* **103**, 207201 (2009).
- [4] S. Pilati, G. Bertainia, S. Giorgini, and M. Troyer, *Phys. Rev. Lett.* **105**, 030405 (2010).
- [5] S.-Y. Chang, M. Randeria, and N. Trivedi, *Proc. Natl. Acad. Sci. USA* **108**, 51 (2010).
- [6] S. Giorgini, J. Boronat, and J. Casulleras, *Phys. Rev. A* **60**, 5129 (1999).
- [7] C. Chin, R. Grimm, P. Julienne, and E. Tiesinga, *Rev. Mod. Phys.* **82**, 1225 (2010).
- [8] A. J. Morris, P. López Ríos, and R. J. Needs, *Phys. Rev. A* **81**, 033619 (2010).
- [9] P. O. Bugnion, J. A. Lofthouse, and G. J. Conduit, *Phys. Rev. Lett.* **111**, 045301 (2013).
- [10] P. O. Bugnion and G. J. Conduit, *Phys. Rev. A* **88**, 013601 (2013).
- [11] P. O. Bugnion and G. J. Conduit, *Phys. Rev. A* **87**, 060502(R) (2013).
- [12] G. J. Conduit and B. D. Simons, *Phys. Rev. Lett.* **103**, 200403 (2009).
- [13] G.-B. Jo *et al.*, *Science* **325**, 1521 (2009).
- [14] D. M. Ceperley and B. J. Alder, *Phys. Rev. Lett.* **45**, 566 (1980).
- [15] C. J. Umrigar, M. P. Nightingale, and K. J. Runge, *J. Chem. Phys.* **99**, 2865 (1993).
- [16] W. M. C. Foulkes, L. Mitás, R. J. Needs, and G. Rajagopal, *Rev. Mod. Phys.* **73**, 33 (2001).
- [17] W. M. C. Foulkes, R. Q. Hood, and R. J. Needs, *Phys. Rev. B* **60**, 4558 (1999).
- [18] G. J. Conduit and B. D. Simons, *Phys. Rev. A* **79**, 053606 (2009).
- [19] H. Zhai, *Phys. Rev. A* **80**, 051605(R) (2009).
- [20] D. L. Maslov and A. V. Chubukov, *Phys. Rev. B* **79**, 075112 (2009).
- [21] A. V. Chubukov and D. L. Maslov, *Phys. Rev. Lett.* **103**, 216401 (2009).
- [22] C. J. Pedder, F. Krüger, and A. G. Green, *Phys. Rev. B* **88**, 165109 (2013).
- [23] R. A. Duine and A. H. MacDonald, *Phys. Rev. Lett.* **95**, 230403 (2005).
- [24] D. L. Maslov and A. V. Chubukov, *Phys. Rev. B* **81**, 045110 (2010).
- [25] U. Karahasanovic, F. Krüger, and A. G. Green, *Phys. Rev. B* **85**, 165111 (2012).
- [26] R. Balian and N. R. Werthamer, *Phys. Rev.* **131**, 1553 (1963).
- [27] D. Fay and J. Appel, *Phys. Rev. B* **22**, 3173 (1980).
- [28] N. D. Mathur *et al.*, *Nature* **394**, 39 (1998).
- [29] R. Roussev and A. J. Millis, *Phys. Rev. B* **63**, 140504(R) (2001).
- [30] G. J. Conduit, C. J. Pedder, and A. G. Green, *Phys. Rev. B* **87**, 121112(R) (2013).
- [31] S. S. Saxena, P. Agarwal, K. Ahilan, F. M. Grosche, R. K. W. Haselwimmer, M. J. Steiner, E. Pugh, I. R. Walker, S. R. Julian, P. Monthoux, G. G. Lonzarich, A. Huxley, I. Sheikin, D. Braithwaite, and J. Flouquet, *Nature (London)* **406**, 587 (2000).

- [32] A. Huxley, I. Sheikin, E. Ressouche, N. Kernavanois, D. Braithwaite, R. Calemczuk, and J. Flouquet, *Phys. Rev. B* **63**, 144519 (2001).
- [33] D. R. Hamann, M. Schlüter, and C. Chiang, *Phys. Rev. Lett.* **43**, 1494 (1979).
- [34] G. B. Bachelet, D. R. Hamann, and M. Schlüter, *Phys. Rev. B* **26**, 4199 (1982).
- [35] D. R. Hamann, *Phys. Rev. B* **40**, 2980 (1989).
- [36] T. Busch, B. G. Englert, K. Rzazewski, and M. Wilkens, *Foundations of Physics* **28**, 549 (1998).
- [37] N. Troullier and J. L. Martins, *Phys. Rev. B* **43**, 1993 (1991).
- [38] A. Zunger and M. L. Cohen, *Phys. Rev. B* **20**, 4082 (1979).
- [39] A. M. Rappe, K. M. Rabe, E. Kaxiras, and J. D. Joannopoulos, *Phys. Rev. B* **41**, 1227 (1990).
- [40] J. S. Lin, A. Qteish, M. C. Payne, and V. Heine, *Phys. Rev. B* **47**, 4174 (1993).
- [41] We provide a Python program to generate the Troullier-Martins, UTP, and square well pseudopotentials at <https://pypi.python.org/pypi/contactpp>.
- [42] J. C. Phillips and L. Kleinman, *Phys. Rev.* **116**, 287 (1959).
- [43] L. Kleinman and J. C. Phillips, *Phys. Rev.* **118**, 1153 (1960).
- [44] B. J. Austin, V. Heine, and L. J. Sham, *Phys. Rev.* **127**, 276 (1962).
- [45] S. Fahy, X. W. Wang, and S. G. Louie, *Phys. Rev. B* **42**, 3503 (1990).
- [46] D. Vanderbilt, *Phys. Rev. B* **41**, 7892 (1990).
- [47] P. E. Blöchl, *Phys. Rev. B* **50**, 17953 (1994).
- [48] F. Serwane, G. Zürn, T. Lompe, T. B. Ottenstein, A. N. Wenz, and S. Jochim, *Science* **332**, 336 (2011).
- [49] G. Zürn, F. Serwane, T. Lompe, A. N. Wenz, M. G. Ries, J. E. Bohn, and S. Jochim, *Phys. Rev. Lett.* **108**, 075303 (2012).
- [50] F. Mohling, *Phys. Rev.* **122**, 1062 (1961).
- [51] R. J. Needs, M. D. Towler, N. D. Drummond, and P. López Ríos, *J. Phys.: Condensed Matter* **22**, 023201 (2010).
- [52] P. López Ríos, A. Ma, N. D. Drummond, M. D. Towler, and R. J. Needs, *Phys. Rev. E* **74**, 066701 (2006).
- [53] N. D. Drummond, M. D. Towler, and R. J. Needs, *Phys. Rev. B* **70**, 235119 (2004).
- [54] G. Rajagopal, R. J. Needs, S. D. Kenny, W. M. C. Foulkes, and A. James, *Phys. Rev. Lett.* **73**, 1959 (1994).
- [55] G. Rajagopal, R. J. Needs, A. James, S. D. Kenny, and W. M. C. Foulkes, *Phys. Rev. B* **51**, 10591 (1995).
- [56] C. Lin, F. H. Zong, and D. M. Ceperley, *Phys. Rev. E* **64**, 016702 (2001).
- [57] G. G. Spink, R. J. Needs, and N. D. Drummond, *Phys. Rev. B* **88**, 085121 (2013).
- [58] F. Mohling, *Phys. Rev.* **122**, 1043 (1961).
- [59] K. Huang and C. N. Yang, *Phys. Rev.* **105**, 767 (1957).